IEEE Access
Multidisciplinary | Rapid Review | Open Access Journal

Received August 2, 2020, accepted August 9, 2020, date of publication August 19, 2020, date of current version September 1, 2020.

Digital Object Identifier 10.1109/ACCESS.2020.3017730

Channel State Information Based Indoor Localization Error Bound Leveraging Pedestrian Random Motion

ZHENYA ZHANG, WEI NIE, YONG WANG, (Member, IEEE), AND LIANGBO XIE, (Member, IEEE)

School of Communication and Information Engineering, Chongqing University of Posts and Telecommunication, Chongqing 400065, China

Corresponding author: Zhenya Zhang (zhenya_cqupt@foxmail.com)

This work was supported in part by the National Natural Science Foundation of China under Grant 61771083, in part by the Chongqing Natural Science Foundation Project under Grant cstc2019jcyj-msxmX0742, and in part by the Postgraduate Scientific Research and Innovation Project of Chongqing under Grant CYS19253.

ABSTRACT Indoor pedestrian motion detection based on the Wi-Fi Received Signal Strength (RSS) has been commonly deployed in recent years. However, the Channel State Information (CSI) based indoor localization methods can be selected to achieve higher localization accuracy since it contains the finer-grained physical-layer information of the signal. Lack of theoretical analysis of the CSI-based error bound that leverages the pedestrian motion posses a challenge to investigate the ideal performance. In this circumstance, this paper proposes the Cramer-Rao Lower Bound (CRLB) concept to derive out the indoor localization error bound leveraging the pedestrian motion that depends on the constructed signal propagation model by considering the relationship between the localization accuracy and the path loss, shadow fading, and multipath effect. Through the experimental comparison, this paper analyzes the difference between the actual localization error and the derived localization error bound, and the impact of different experimental parameters on the localization performance is analyzed, as well as discusses the influence of the asynchronous effect between the transmitter and the receiver on the performance of the proposed localization error bound. The experimental results show that the derived error bound has the same trend as the actual error, which validate our theoretical analysis.

INDEX TERMS Indoor localization, channel state information, pedestrian motion, CRLB, asynchronous effect.

I. INTRODUCTION

The complexity of the indoor layout results in the signal fading caused by the obstacle and pedestrian motion, thus the widely used Global Positioning System (GPS) [1] is unable to meet the accuracy requirement of most of the indoor Location-based Service (LBS) [2]. In recent years, Many scholars have carried out a series of research on indoor localization technology and proposed a variety of indoor localization methods according to the different signal sources, such as Bluetooth [3], Radio Frequency Identification (RFID) [4], [5], ZigBee [6], Ultra Wide Band (UWB) [7], and Wi-Fi [8] indoor localization method. The biggest advantage of Bluetooth indoor localization technology is the small size of the device, low power consumption, and easy to integrate in mobile devices such as mobile phones. However, for complex indoor environments, Bluetooth indoor localization technology is seriously interfered by noise, and the price of Bluetooth devices is relatively expensive. The indoor localization technology based on RFID can achieve centimeter-level localization accuracy, and lower cost. However, RFID is not easy to integrate into mobile devices and has a short working distance [9], [10]. As a low-power and low-cost localization method, ZigBee indoor localization technology has very high working efficiency, but ZigBee's signal transmission is seriously interfered by multipath effects and pedestrian motion, and excessively depends on the accuracy of the localization algorithm. Compared with the traditional localization systems, the UWB localization system has the advantages of stronger penetration, better

The associate editor coordinating the review of this manuscript and approving it for publication was Mu Zhou.

anti-multipath effect, higher safety, and higher-precision localization. However, its power consumption is higher, and it needs to be arranged in advance. Compared with the above localization methods, Wi-Fi indoor localization technology based on Received Signal Strength (RSS) [11] have become the mainstream of indoor localization technology due to its wide signal coverage, low hardware requirements and simple network deployment. However, due to its susceptibility to multi-path effects and its poor stability, the application of localization technology based on RSS in the actual indoor environment is greatly restricted. In comparison with often Wi-Fi based on RSS, the CSI achieves higher localization accuracy due to finer-grained physical-layer information of the signal [12]. At present, indoor localization technology based on CSI have deployed in various applications such as indoor localization, intrusion detection, path planning in large-scale indoors and underground parking lots [13]–[16].

The CSI-based localization methods leveraging the pedestrian motion are relatively mature, but there is a lack of the related theoretical analysis of the indoor localization error bound, which makes it challenging to investigate these methods ideal localization performance. Meanwhile, the asynchronous effect of hardware equipment is one of the main factors affecting the CSI-based localization accuracy [17], [18] and it is incurred by the crystal oscillating circuits in different devices and will incur a sampling time offset or sampling frequency offset. To summarize, the two main contributions of this paper are listed as follows.

- The concept of the Cramer-Rao Lower Bound (CRLB) in the frequency domain is used to analyze the CSI-based localization error bound leveraging the pedestrian motion.
- By considering the relationship between the localization accuracy and the path loss, shadow fading, multipath effect, and asynchronous effect, the CSI-based localization error bound leveraging the pedestrian motion is derived out.

The rest of this paper is organized as follows. Some related works on indoor localization methods based on pedestrian motion, localizaiton error bound and some factors affecting localization accuracy are surveyed in Section II. The proposed approach is described in detail in Section III, The problem formulation and solution is shown in IV and V, and then Section VI shows the related experimental results. Finally, Section VII concludes this paper.

II. RELATED WORK

Due to the rich physical layer information and high stability of the CSI, more and more scholars have conducted research on indoor localization methods based on pedestrian motion. Authors in [14] propose a device-free human tracking system only using existing commercial WiFi supported devices, which consider a human walking trajectory consists of a series of moving behaviors and determine the trajectory by detect those behaviors. Authors in [19] present an accurate device-free passive indoor location tracking system that adopts channel state information (CSI) and use the fine-grained subchannel measurements for multiple input multiple output (MIMO) orthogonal frequency-division multiplexing physical layer parameters to improve localization and tracking accuracy. Authors in [20] propose a CSI-based indoor tracking system which combines velocity estimation to track human trajectory. Authors in [21] analyze the sensitivity of CSI and achieve location matching by quadratic discriminant analysis to classify CSI fingerprints. Authors in [22] propose a new passive human trajectory tracking algorithm based on the channel state information (CSI) in indoor environment to support many applications with the elder health care.

In the process of wireless signal propagation, the attenuation of signal strength is mainly caused by three factors: multipath fading, path loss, shadowing. Due to the multipath effect, each signal component will reach the receiver through different paths during the propagation process, and then these different signal components superimpose each other to cause interference, which distorts the original signal. The path loss refers to the signal loss caused by the signal propagation distance and channel characteristics. And the shadowing is that signal power loss caused by the shadow effect caused by the blocking of the building on the propagation path. [23]–[25].

When using CSI for localizaiton, the transmitter uses Orthogonal Frequency Division Multiplexing (OFDM) technology to send data in parallel on multiple orthogonal subcarriers and demodulate at the receivers, but due to asynchronous effects (such as Carrier Frequency Offset (CFO) and the clock asynchronization) [26], it is difficult to ensure the orthogonality of the receiving subcarriers, so the performance of CSI-based indoor Wi-Fi localization method will decrease due to the impact of Inter Symbol Interference (ISI) and Inter Carrier Interference (ICI).

As a key part of the indoor Wi-Fi localization technology based on CSI, OFDM technology needs to use an effective synchronization mechanism to ensure the efficiency and reliability of the modulation process, so the analysis of asynchronous effects in OFDM technology is particularly important. Therefore, Authors in [27] propose a blind carrier frequency offset estimator for OFDM systems based on the frequency analysis of the received signal, and derives a closed-form CFO estimate. Authors in [28] propose a cost-effective sampling frequency offset (SFO) compensation scheme based on a simple training symbol (TS) and experimentally demonstrate in an OFDM transmission system. Authors in [29] propose a CFO compensation algorithm based on preamble, and combine with OFDM model to solve the problem of energy loss and distortion of the received signal caused by CFO. Authors in [30] propose a maximum likelihood method for jointly estimating carrier frequency offset and sampling frequency offset in receivers for orthogonal frequency division multiplexing signals. In the indoor Wi-Fi localization process based on CSI, the existing asynchronous effects when using OFDM technology to modulate Wi-Fi signals will lead to a decrease in localization

accuracy. Therefore, it is necessary to analyze the impact of asynchronous effects on localization performance, and to improve the effectiveness and robustness of the localization system.

Although the CSI-based localization method leveraging the pedestrian motion is relatively mature, there is a general lack of theoretical analysis on the localization error bound. To the best of our knowledge, most of the studies on the indoor localization error bound are based on the concept of the Cramer-Rao Lower Bound (CRLB) [31]–[34]. For example, Authors in [31] use an information-theoretic lens to view the error bound of wireless local area network localization, which is recognized as one of the superior candidate localization techniques in the GPS-denied environment. Authors in [32] uses Fisher information matrix (FIM) to derive the localization error bounds under different signal distributions to evaluate the error bound of RSS-based indoor localizaiton systems. Authors in [33] rely on an indoor signal propagation model considering the multi-path effect to analyze the impact of shadow fading and the anchor node number on the CSI-based indoor localization error bound. Authors in [34] investigate the relationship between the CSI-based indoor localization error bound and the signal propagation delay and the antenna number from the perspective of the frequency domain. However, the current studies on the indoor localization error bound based on the CRLB rarely consider the pedestrian motion.

In this paper, considering the relationship between the indoor localization error bound and the environment factor such as the path loss, multi-path effect, noise and the device factor such as the AP number, AP locations, bandwidth and asynchronous effect, we derive and propose the closed-form solution to the CSI-based indoor localization error bound leveraging the pedestrian motion, which can be used to investigate the ideal performance of the existing indoor localization methods when the pedestrian is moving.

III. SYSTEM MODEL

A. SIGNAL MODEL

CSI considered as the physical-layer information of the signal, contains the amplitude and phase information of each subcarrier that can be used to describe the attenuation and frequency deviation characteristics of the signal propagating from the transmitter to the receiver. The signal amplitude attenuation occurs during the propagation process, and it is also affected by the multi-path effect due to obstacles such as the floor, wall, and ceiling [35]. Meanwhile, by considering slow speed pedestrian movement within the indoor environment, the Doppler frequency deviation of the signal ranging within 10-20 Hz can be ignored. Thus, the waveform of the received signal in the time domain can be represented as

$$r(t) = \sum_{i=1}^{l} a^{(i)} s(t - \tau^{(i)}) + z(t) \tag{1}$$

where $s(t)$ is the transmitted signal waveform, l is the propagation paths number, $a^{(i)}$ and $\tau^{(i)}$ is the i-th propagation path for the amplitude and propagation delay of the received signal respectively. $z(t)$ is the noise following the Gaussian distribution with the mean 0 and variance δ^2. After conducting the Analog-to-Digital Converter (ADC) transformation, the waveform of the received signal is converted into

$$r(nT) = \sum_{i=1}^{l} a^{(i)} s(nT - \tau^{(i)}) + z(nT) \tag{2}$$

where $n = 1, \cdots, L$, T is the sampling period and L is the number of sampling points. Based on this, the waveform of the received signal at the m-th ($m = 1, \cdots, N$) Access Point (AP) can be represented as

$$r_m(nT) = \sum_{i=1}^{l} a_m^{(i)} s(nT - \tau_m^{(i)}) + z(nT) \tag{3}$$

where $n = 1, \cdots, L$, $a_m^{(i)}$ and $\tau_m^{(i)}$ are the amplitude and propagation delay of the received signal respectively on the i-th propagation path at the m-th AP. Conducting the L-point Discrete Fourier Transform (DFT) of $r_m(nT)$, the corresponding waveform of the received signal in the frequency domain can be obtained as

$$R_m(k) = \sum_{i=1}^{l} a_m^{(i)} S(k) e^{\frac{-j2\pi k \tau_m^{(i)}}{LT}} + \eta(k) \tag{4}$$

where $k = 0, \cdots, L-1$, $S(k)$ and $\eta(k)$ are the power spectrums of the transmitted signal and the noise following the Gaussian distribution with the mean 0 and covariance $L\delta^2$ respectively.

B. LOCALIZATION ERROR BOUND MODEL

According to the Fisher information theory [36], the CRLB is defined as the inverse of the Fisher Information Matrix (FIM), which describes the variance of the estimated value of unknown parameters. The FIM in the time domain can be expressed as

$$J(\boldsymbol{\theta}) = -E\left(\frac{\partial^2}{\partial\theta_i \partial\theta_j} \ln f(\boldsymbol{\theta})\right) \tag{5}$$

where θ_i and θ_j are the unknown parameters in the parameter $\boldsymbol{\theta}$ to be estimated respectively, $f(\boldsymbol{\theta})$ is Probability Density Function (PDF) of $\boldsymbol{\theta}$, E is expectation operation, the mean square error matrix can be calculated from FIM inequality [32], [33] as

$$var\left(\widehat{\boldsymbol{\theta}}\right) = E\left(\left(\widehat{\boldsymbol{\theta}} - \boldsymbol{\theta}\right)\left(\widehat{\boldsymbol{\theta}} - \boldsymbol{\theta}\right)^{\mathrm{T}}\right) \geq J(\boldsymbol{\theta})^{-1} \tag{6}$$

where $\widehat{\boldsymbol{\theta}}$ is the estimated value of $\boldsymbol{\theta}$ and $J(\boldsymbol{\theta})^{-1}$ is CRLB of $\boldsymbol{\theta}$. We set the vector of parameters to be estimated as the 2-dimensional (2-D) coordinate of the pedestrian $\boldsymbol{\theta} = (\theta_1, \theta_2)^{\mathrm{T}}$, the mean square error matrix can be calculated as

$$\begin{aligned} var\left(\widehat{\boldsymbol{\theta}}\right) &= E\left\{\left(\widehat{\boldsymbol{\theta}} - \boldsymbol{\theta}\right)\left(\widehat{\boldsymbol{\theta}} - \boldsymbol{\theta}\right)^{\mathrm{T}}\right\} \\ &= \begin{bmatrix} \sigma_1^2 & \sigma_{12} \\ \sigma_{21} & \sigma_2^2 \end{bmatrix} \geq J(\theta)^{-1} \end{aligned} \tag{7}$$

where $\sigma_1^2 = E\left(\widehat{\theta}_1 - \theta_1\right)^2 \left(\geq J_{22}/|J(\boldsymbol{\theta})|\right)$ and $\sigma_2^2 = E\left(\widehat{\theta}_2 - \theta_2\right)^2 \left(\geq J_{11}/|J(\boldsymbol{\theta})|\right)$ are the mean square error of θ_1 and θ_2 respectively, and $\sigma_{12} = E\left\{\left(\widehat{\theta}_1 - \theta_1\right)\left(\widehat{\theta}_2 - \theta_2\right)^{\mathrm{T}}\right\}$ $\left(\geq J_{12}/|J(\boldsymbol{\theta})|\right)$ and $\sigma_{21} = E\left\{\left(\widehat{\theta}_2 - \theta_2\right)\left(\widehat{\theta}_1 - \theta_1\right)^{\mathrm{T}}\right\}$ $\left(\geq J_{21}/|J(\boldsymbol{\theta})|\right)$ are covariance of $\widehat{\theta}_1$ and $\widehat{\theta}_2$, $\widehat{\theta}_2$ and $\widehat{\theta}_1$ respectively. The FIM with respect to $\boldsymbol{\theta}$ can be expressed as

$$J(\boldsymbol{\theta}) = \begin{bmatrix} J_{11} & J_{12} \\ J_{21} & J_{22} \end{bmatrix} \tag{8}$$

where $J_{11} = -E\left(\frac{\partial^2}{\partial {\theta_1}^2} \ln f\left(\boldsymbol{\theta}\right)\right)$, $J_{22} = -E\left(\frac{\partial^2}{\partial {\theta_2}^2} \ln f\left(\boldsymbol{\theta}\right)\right)$, and $J_{12} = J_{21} = -E\left(\frac{\partial^2}{\partial \theta_1 \partial \theta_2} \ln f\left(\boldsymbol{\theta}\right)\right)$. Based on this, the error bound equals to

$$V_\theta = \frac{J_{11} + J_{22}}{J_{11}J_{22} - J_{12}^2} \tag{9}$$

Different from the previous studies on the CSI-based indoor localization error bound using the time-domain model [32], we rely on the frequency-domain model shown in (4), to derive out the error bound with the benefit of making the waveform information consistent with the practical capability of the Intel 5300 toolkit used for receiving the CSI and avoiding the problem that the FIM of the parameter to be estimated cannot be obtained due to the PDF of the parameter to be estimated is not available in the time domain. To achieve this goal, we set the expectation of the vector of $\boldsymbol{X} = (R_m(0), \cdots, R_m(L-1))^{\mathrm{T}}$ as $\boldsymbol{\mu} = \left(\overline{R_m(0)}, \cdots, \overline{R_m(L-1)}\right)^{\mathrm{T}}$ and the vector of parameters to be estimated as the 2-dimensional (2-D) coordinate of the pedestrian $\boldsymbol{\theta} = (\theta_1, \theta_2)^{\mathrm{T}}$, where $\overline{R_m(k)}$ is the expectation of $R_m(k)$ and T is the transpose operation. The element on the i-th row and j-th column in the FIM with respect to $\boldsymbol{\theta}$ is then calculated as [36]

$$I_{ij} = 2\mathrm{Re}\left[\frac{\partial \boldsymbol{\mu}^{\mathrm{H}}}{\partial \theta_i} \boldsymbol{\Sigma}^{-1} \frac{\partial \boldsymbol{\mu}}{\partial \theta_j}\right], \quad i, j = 1, 2 \tag{10}$$

where Re and H are real-part and matrix conjugate transpose operations, $\boldsymbol{\Sigma} = L\delta^2 \boldsymbol{E}$ is the covariance matrix of $\boldsymbol{X}$, and $\boldsymbol{E}$ is identitiy matrix. Based on this, the error bound equals to

$$V'_\theta = \frac{I_{11} + I_{22}}{I_{11}I_{22} - I_{12}^2} \tag{11}$$

IV. CRLB FOR LOCATION ESTIMATION

The waveform of the received signal at the m-th AP from the pedestrian movement by the moment t from (1) can be represented as

$$y_m(t) = \sum_{i=1}^{l} a_{t,m}^{(i)} s(t - \tau_{t,m}^{(i)}) + z(t) \tag{12}$$

where $a_{t,m}^{(i)}$ and $\tau_{t,m}^{(i)}$ are the amplitude and the propagation delay of the received signal respectively on the i-th propagation path at the m-th AP by the moment t. In this case, the vector of parameters to be estimated by the moment t can be constructed as $\boldsymbol{\theta'} = \left(a_{t,1}^{(1)}, \tau_{t,1}^{(1)}, \cdots, a_{t,1}^{(l)}, \tau_{t,1}^{(l)}, \cdots, a_{t,N}^{(1)}, \tau_{t,N}^{(1)}, \cdots, a_{t,N}^{(l)}, \tau_{t,N}^{(l)}\right)$.

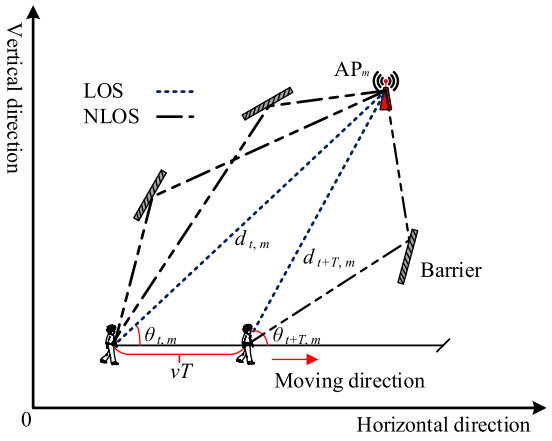

FIGURE 1. Geometrical relationship between the m-th AP and pedestrian locations by moments t and $t+T$.

To derive out the CSI-based indoor localization error bound considering the pedestrian motion at every two consecutive moments, we propose the association of parameters. Firstly, we set 2-D coordinates of the pedestrian by the moment t and the m-th AP as (x_t, y_t) and (x_m, y_m) respectively, then we calculate the inter distance as $d_{t,m} = \sqrt{(x_t - x_m)^2 + (y_t - y_m)^2}$. Since the signal-sampling rate is much higher than the step rate of the pedestrian, we have $\theta_{t,m} \approx \theta_{t+T,m}$, where $\theta_{t,m}$ and $\theta_{t+T,m}$ are the horizontal angles of directions from pedestrian locations by moments t and $t+T$ to the m-th AP respectively. Based on this, the distance between pedestrian locations by moments t and $t+T$ can be derived as $d_{t,t+T} = vT \approx \left|d_{t,m} - d_{t+T,m}\right| \cos\theta_{t,m}$, then we can obtain $d_{t,m} \approx vT\cos\theta_{t,m} + d_{t+T,m}$, where v is is the moving speed of the pedestrian, as shown in Fig. 1.

To characterize multipath propagation, we need to consider the propagation process of multipath signals. Since the propagation distance of multipath signals cannot be obtained accurately, we use weighted methods to represent the propagation delay of multipath signals as much as possible, according to the random weighting theory [33], we have

$$\begin{aligned} \tau_{t,m}^{(i)} &= \frac{\lambda_m^i d_{t,m}}{c} \approx \frac{\lambda_m^i \left(vT\cos\theta_{t,m} + d_{t+T,m}\right)}{c} \\ &= \frac{\lambda_m^i \left(vT\cos\theta_{t,m} + \sqrt{(x_{t+T} - x_m)^2 + (y_{t+T} - y_m)^2}\right)}{c} \end{aligned} \tag{13}$$

where c is the speed of light, λ_m^i is the weighting factor of the i-th propagation path at the m-th AP.

Due to the small-scale fading caused by the multipath effect is negligible in the indoor environment, the amplitude

attenuation during signal propagation is only related to the distance. Specifically, the equipment used in the CSI positioning process is basically equipped with multiple antennas [17], [37], so it can be explained that the propagation waveform can be modeled as a spherical wave, that is, the signal amplitude is inversely proportional to the signal propagation distance. Then we have

$$a_{t,m}^{(i)} = \frac{a_0}{\lambda_m^i d_{t,m}} \varepsilon^{p_m^i} \approx \frac{a_0}{\lambda_m^i \left(vT\cos\theta_{t,m} + d_{t+T,m}\right)} \varepsilon^{p_m^i} = \frac{a_0}{\lambda_m^i \left(vT\cos\theta_{t,m} + \sqrt{(x_{t+T}-x_m)^2 + (y_{t+T}-y_m)^2}\right)} \varepsilon^{p_m^i} \tag{14}$$

where a_0 is the amplitude of the received signal at 1 m from the transmitter (reference location), ε ($\in (0, 1)$) is the environment coefficient, and p_m^i is the number of reflections of the signal on the i-th propagation path at the m-th AP.

According to (13) and (14), we can find that the estimation of $\boldsymbol{\theta'}$ is equivalent to the estimation of $\boldsymbol{\theta} = (x_{t+T}, y_{t+T})$, then the waveform of the received signal at the m-th AP by the moment t can be represented as

$$y_m(t) = \sum_{i=1}^{l} \frac{a_0}{\lambda_m^i d_{t,m}} \varepsilon^{p_m^i} s(t - \frac{\lambda_m^i d_{t,m}}{c}) + z(t) \tag{15}$$

By conducting the L-point DFT of $y_m(t)$, the corresponding frequency domain can be obtained as

$$Y_m(k) \approx \sum_{i=1}^{l} \frac{a_0 \varepsilon^{p_m^i}}{\lambda_m^i d_{t,m}} S(k) e^{\frac{-j2\pi k \lambda_m^i d_{t,m}}{LTc}} + \eta(k) \tag{16}$$

From (10), by setting the expectation of the vector of observations $\boldsymbol{X} = \left(Y_1^{(1)}(0), \cdots, Y_1^{(1)}(L-1), \cdots, Y_N^{(l)}(0), \cdots, Y_N^{(l)}(L-1)\right)^{\mathrm{T}}$ as $\mu = \left(\overline{Y_1^{(1)}(0)}, \cdots, \overline{Y_1^{(1)}(L-1)}, \cdots, \overline{Y_N^{(l)}(0)}, \cdots, \overline{Y_N^{(l)}(L-1)}\right)^{\mathrm{T}}$, where $Y_m^{(i)}(k)$ is the observation on the i-th propagation path at the m-th AP and $\overline{Y_m^{(i)}(k)}$ is the expectation of $Y_m^{(i)}(k)$, the FIM with respect to $\boldsymbol{\theta}$ is constructed as

$$\boldsymbol{I}_{\boldsymbol{\theta}} = \frac{2}{L\sigma^2} \begin{bmatrix} I_{xx} & I_{xy} \\ I_{yx} & I_{yy} \end{bmatrix} = \frac{2a_0^2}{L\delta^2} \sum_{m=1}^{M} H_m \boldsymbol{D}_m \tag{17}$$

where

$$H_m = \sum_{i=1}^{l} \sum_{k=0}^{L-1} |S(k)|^2 \left(\frac{1}{d_{t,m}^4 \left(\frac{\lambda_m^i}{\varepsilon^{p_m^i}}\right)^2} + \frac{4\pi^2 k^2}{L^2 c^2 T^2 d_{t,m}^2 \left(\frac{1}{\varepsilon^{p_m^i}}\right)^2}\right) \tag{18}$$

$$\boldsymbol{D}_{t,m} = \begin{bmatrix} \cos^2\theta_{t,m} & cos\theta_{t,m}\sin\theta_{t,m} \\ \sin\theta_{t,m} cos\theta_{t,m} & \sin^2\theta_{t,m} \end{bmatrix} \tag{19}$$

and $|S(k)|$ is the amplitude of the transmitted signal.

Finally, the CSI-based indoor localization error bound leveraging the pedestrian motion is derived as (20), as shown at the bottom of the page.

V. ASYNCHRONOUS EFFECT ANALYSIS

A. ERROR BOUND UNDER THE CLOCK ASYNCHRONOUS EFFECT

The asynchronous clock effect caused by the clock deviation between the target and AP will bring the phase deviation of the frequency domain signal, which will affect the signal demodulation result and increase the bit error rate. Specifically, the phase deviation of the frequency domain signal introduced by the difference in hardware devices will cause the sampling time of the target and the AP to be out of sync, which in turn causes a fixed time offset τ_0 between the actual sampling time of the AP and the optimal sampling time [34], [38].

According to (12), (13) and (14), we represent the waveform of the received signal with the clock asynchronous effect at the m-th AP by the moment t under the pedestrian motion as

$$\tilde{y}_m(t) = \sum_{i=1}^{l} a_{t,m}^{(i)} s(t - \tau_{t,m}^{(i)} - \tau_0) + z(t) \tag{21}$$

By conducting the L-point DFT of $\tilde{y}_m(t)$, the corresponding frequency domain can be obtained as

$$\tilde{Y}_m(k) \approx \sum_{i=1}^{l} \frac{a_0 \varepsilon^{p_m^i}}{\lambda_m^i d_{t,m}} S(k) e^{\frac{-j2\pi k \left(\lambda_m^i d_{t,m} + c\tau_0\right)}{LTc}} + \eta(k) \tag{22}$$

In this case, the vector of parameters to be estimated by the moment t can be obtained as $\tilde{\boldsymbol{\theta}} = \left(a_{t,1}^{(1)}, \tau_{t,1}^{(1)}, \cdots, a_{t,1}^{(l)}, \tau_{t,1}^{(l)}, \cdots, a_{t,N}^{(1)}, \tau_{t,N}^{(1)}, \cdots, a_{t,N}^{(l)}, \tau_{t,N}^{(l)}, \tau_0\right)$. There are not only the to be estimated parameters x_{t+T} and y_{t+T} for the target position estimation, but also the time offset τ_0 caused by the clock asynchronous effect. Similarly, according to (10), the FIM with respect to $\tilde{\boldsymbol{\theta}}$ is constructed as

$$\mathbf{I}_{\tilde{\boldsymbol{\theta}}} = \begin{bmatrix} \mathbf{A} & \mathbf{B} \\ \mathbf{B}^{\mathbf{T}} & \mathbf{C} \end{bmatrix} \tag{23}$$

where

$$\mathbf{A} = \begin{bmatrix} \sum_{m=1}^{M} H_m \cos\theta_{t,m}^2 & \sum_{m=1}^{M} H_m \cos\theta_{t,m}\sin\theta_{t,m} \\ \sum_{m=1}^{M} H_m \sin\theta_{t,m}\cos\theta_{t,m} & \sum_{m=1}^{M} H_m \sin\theta_{t,m}^2 \end{bmatrix} \tag{24}$$

$$V_{\boldsymbol{\theta}} = \frac{L\delta^2}{2a_0^2} \frac{\sum_{m=1}^{N} H_m}{\left(\sum_{m=1}^{N} H_m \cos^2\theta_{t,m}\right)\left(\sum_{m=1}^{N} H_m \sin^2\theta_{t,m}\right) - \left(\sum_{m=1}^{N} H_m \cos\theta_{t,m}\sin\theta_{t,m}\right)^2} \tag{20}$$

$$\mathbf{B} = \left[\sum_{m=1}^{M} \frac{J_m \cos\theta_{t,m}}{v} \quad \sum_{m=1}^{M} \frac{J_m \sin\theta_{t,m}}{v} \right]^{\mathrm{T}} \tag{25}$$

$$\mathbf{C} = \sum_{m=1}^{M} J_m \tag{26}$$

where $J_m = \sum_{i=1}^{l} \sum_{k=1}^{L-1} |S(k)|^2 \frac{4\pi^2 (\varepsilon^{p_m^i})^2 k^2}{(\lambda_m^i)^2 d_{t,m}^2 L^2 T^2}$.

However, we are only interested in the location information of the target, which can be obtained with equivalent Fisher information matrix (EFIM).

According to [39], construct EFIM about $\tilde{\boldsymbol{\theta}}$ as

$$\mathbf{I}_E = \mathbf{A} - \mathbf{B}\mathbf{C}^{-1}\mathbf{B}^{\mathbf{T}} \tag{27}$$

which has the property that $\left[\mathbf{I}_{\tilde{\boldsymbol{\theta}}}^{-1}\right]_{2\times 2} = \mathbf{I}_E^{-1}$, where $[\cdot]_{n\times n}$ is the submatrix of the first n rows and first n columns of the matrix, the CSI-based indoor localization error bound with asynchronous effect leveraging the pedestrian motion is derived as

$$V_{\tilde{\boldsymbol{\theta}}} = \mathrm{tr}\left\{\mathbf{I}_E^{-1}\right\} = \frac{L\delta^2}{2a_0^2} \frac{I_4}{I_1 I_2 - {I_3}^2} \tag{28}$$

where

$$I_1 = \sum_{m=1}^{N} H_m \cos^2(\theta_m) - \frac{\left(\sum_{m=1}^{N} J_m \cos\theta_m\right)^2}{c^2 \sum_{m=1}^{N} J_m},$$

$$I_2 = \sum_{m=1}^{N} H_m \sin^2(\theta_m) - \frac{\left(\sum_{m=1}^{N} J_m \sin\theta_m\right)\left(\sum_{m=1}^{N} J_m \sin\theta_m\right)}{c^2 \sum_{m=1}^{N} J_m},$$

$$I_3 = \sum_{m=1}^{N} H_m \sin\theta_m \cos\theta_m - \frac{\left(\sum_{m=1}^{N} J_m \cos\theta_m\right)\left(\sum_{m=1}^{N} J_m \sin\theta_m\right)}{c^2 \sum_{m=1}^{N} J_m},$$

$$I_4 = \sum_{m=1}^{N} H_m - \frac{\left(\sum_{m=1}^{N} J_m \cos\theta_m\right)^2 + \left(\sum_{m=1}^{N} J_m \sin\theta_m\right)^2}{c^2 \sum_{m=1}^{N} J_m}.$$

B. ERROR BOUND WITH THE CARRIER FREQUENCY OFFSET

According to [40], the CFO is caused by the difference between the receiver oscillator and the transmitter oscillator and the doppler frequency shift. The phase noise introduced by the channel nonlinearity and the phase shift caused by the CFO will destroy the orthogonality of subcarriers. The CFO is unpredictable, but can be regarded as a constant during a short-time measurement. We set f is frequency shift caused by the CFO, then received signal after DFT with CFO at the m-th AP by the moment t under the pedestrian motion as

$$Y'_m(k) \approx \sum_{i=1}^{l} \frac{a_0 \varepsilon^{p_m^i}}{\lambda_m^i d_{t,m}} S(k-f) e^{\frac{-j2\pi(k-f)\lambda_m^i d_{t,m}}{LTc}} + \eta(k) \tag{29}$$

In this case, the vector of parameters to be estimated by the moment t can be obtained as $\boldsymbol{\theta}'' = \left(a_{t,1}^{(1)}, \tau_{t,1}^{(1)}, \cdots, a_{t,1}^{(l)}, \tau_{t,1}^{(l)}, \cdots, a_{t,N}^{(1)}, \tau_{t,N}^{(1)}, \cdots, a_{t,N}^{(l)}, \tau_{t,N}^{(l)}, f\right)$. Similarly, there are not only the to be estimated parameters x_{t+T} and y_{t+T} for the target position estimation, but also the frequency shift f caused by CFO. Similarly, according to (5), the FIM with respect to $\boldsymbol{\theta}''$ is constructed as

$$\mathbf{I}_{\tilde{\boldsymbol{\theta}}} = \begin{bmatrix} \mathbf{E} & \mathbf{F} \\ \mathbf{F}^{\mathbf{T}} & \mathbf{G} \end{bmatrix} \tag{30}$$

where

$$\mathbf{E} = \begin{bmatrix} \sum_{m=1}^{M} P_m \cos^2\theta_{t,m} & \sum_{m=1}^{M} P_m \cos\theta_{t,m} \sin\theta_{t,m} \\ \sum_{m=1}^{M} P_m \sin\theta_{t,m} \cos\theta_{t,m} & \sum_{m=1}^{M} P_m \sin^2\theta_{t,m} \end{bmatrix} \tag{31}$$

$$\mathbf{F} = \left[\sum_{m=1}^{M} Z_m \cos\theta_{t,m} \quad \sum_{m=1}^{M} Z_m \sin\theta_{t,m} \right]^{\mathrm{T}} \tag{32}$$

$$\mathbf{G} = \sum_{m=1}^{M} U_m \tag{33}$$

where the values of P_m, Z_m and U_m are as follows (34), as shown at the bottom of the next page.

Similarly, we are only interested in the location information of the target, which can be obtained with equivalent Fisher information matrix (EFIM). We can construct EFIM about $\tilde{\boldsymbol{\theta}}$ as

$$\mathbf{I}_E = \mathbf{E} - \mathbf{F}\mathbf{G}^{-1}\mathbf{F}^{\mathbf{T}} \tag{35}$$

According to $\left[\mathbf{I}_{\tilde{\boldsymbol{\theta}}}^{-1}\right]_{2\times 2} = \mathbf{I}_E^{-1}$, the CSI-based indoor localization error bound with CFO leveraging the pedestrian motion is derived as

$$V_{\theta''} = \mathrm{tr}\left\{\mathbf{I}_E^{-1}\right\} = \frac{L\delta^2}{2a_0^2} \frac{\chi_4}{\chi_1 \chi_2 - \chi_3^2} \tag{36}$$

where the values of χ_1, χ_2, χ_3 and χ_4 are as follows (37), as shown at the bottom of the next page.

VI. EXPERIMENTAL RESULTS

The real indoor experiment is conducted in a 49.3 m by 17.8 m as in Fig. 2 to evaluate localization error bounds corresponding to 5 different motion paths and compare them with the actual localization errors. The setup comprises of randomly deployed 7 Intel 5300 toolkit APs to receipt the CSI from the TP-LINK TL-WR2041N transmitter carried by the moving pedestrian. Especially to deserve to be mentioned, we use the method of controlling variables to observe the influence of different parameters on the error bound and actual error. The main parameters in the simulation are listed in table 1.

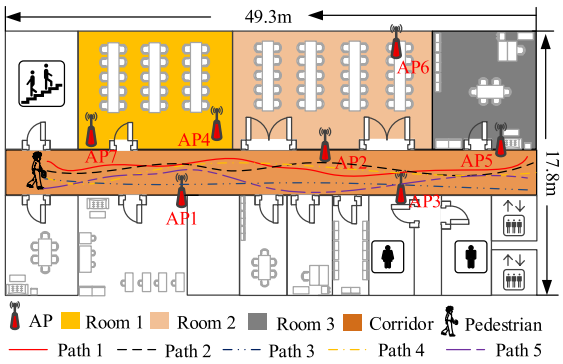

FIGURE 2. Environmental layout.

TABLE 1. The main parameter in the simulation.

The parameter	Value
a_0	default -40dBm
i	range from 1 to 3
λ_m^i	range from 1.2 to 20
ε	range from 0 to 1
δ^2	-95, -90, -85, -80 or -75dBm; default -75dBm
AP number	3, 4, 5, 6 or 7; default 3
Bandwidth	60, 80, 120, 200 or 300MHz; default 60MHz
Path number	1, 2, 3, 4 or 5; default 3

A. IMPACT OF DIFFERENT PARAMETERS ON ERROR BOUND

Experimental evaluation for the proposed theoretical analysis is carried out by analysing parameters such as the pedestrian motion, the AP's density impact, the noise power, and the bandwidth. From the observation of the Cumulative Density Function (CDF) curve in Fig. 3, we observe a distinct difference between the relationship trend for the error bound and the actual error towards localization of each pedestrian motion path. This is due to the reason that the localization error bound is obtained by the assumption of the ideal CSI acquisition, signal propagation modelling, and parameters estimation, which are impossible to be satisfied in the real indoor environment. However, the variation trend of the CDFs is much the same, which demonstrates the effectiveness of the derived and proposed localization error bound leveraging the pedestrian motion.

$$\begin{cases} P_m = \sum_{i=1}^{l}\sum_{k=1}^{L-1}\left[\frac{\left(\varepsilon^{p_m^i}\right)^2 S(k-f)}{\left(\lambda_m^i d_{t,m}\right)^3}\left|\frac{\partial S(k-f)}{\partial(k-f)}\right| + \frac{\left(\varepsilon^{p_m^i}\right)^2 4\pi^2 (k-f)\,|S(k-f)|^2}{\lambda_m^i d_{t,m} L^2 T^2 c^2}\right] \\ U_m = \sum_{i=1}^{l}\sum_{k=1}^{L-1}\left[\left(\frac{\varepsilon^{p_m^i}}{\lambda_m^i d_{t,m}}\right)^2\left|\frac{\partial\,|S(k-f)|}{\partial(k-f)}\right| + \frac{4\pi^2\left(\varepsilon^{p_m^i}\right)^2 |S(k-f)|^2}{L^2T^2c^2}\right] \\ Z_m = \sum_{i=1}^{l}\sum_{k=1}^{L-1}|S(k-f)|^2\left[\frac{\left(\varepsilon^{p_m^i}\right)^2}{\left(\lambda_m^i d_{t,m}\right)^4} + \frac{4\pi^2(k-f)^2}{\left(\lambda_m^i d_{t,m}\right)^2 L^2T^2c^2}\right] \end{cases} \tag{34}$$

$$\begin{cases} \chi_1 = \sum_{m=1}^{N} P_m - \frac{\left(\sum_{m=1}^{N} Z_m \cos\theta_{t,m}\right)^2 + \left(\sum_{m=1}^{N} Z_m sin\theta_{t,m}\right)^2}{\sum_{m=1}^{N} U_m} \\ \chi_2 = \sum_{m=1}^{N} P_m \cos\theta_{t,m}^2 - \frac{\left(\sum_{m=1}^{N} Z_m \cos\theta_{t,m}\right)^2}{\sum_{m=1}^{N} U_m} \\ \chi_3 = \sum_{m=1}^{N} P_m sin\theta_{t,m}^2 - \frac{\left(\sum_{m=1}^{N} Z_m sin\theta_{t,m}\right)^2}{\sum_{m=1}^{N} U_m} \\ \chi_4 = \sum_{m=1}^{N} P_m cos\theta_{t,m} sin\theta_{t,m} - \frac{\left(\sum_{m=1}^{N} Z_m \cos\theta_{t,m}\right)\left(\sum_{m=1}^{N} Z_m sin\theta_{t,m}\right)}{\sum_{m=1}^{N} U_m} \end{cases} \tag{37}$$

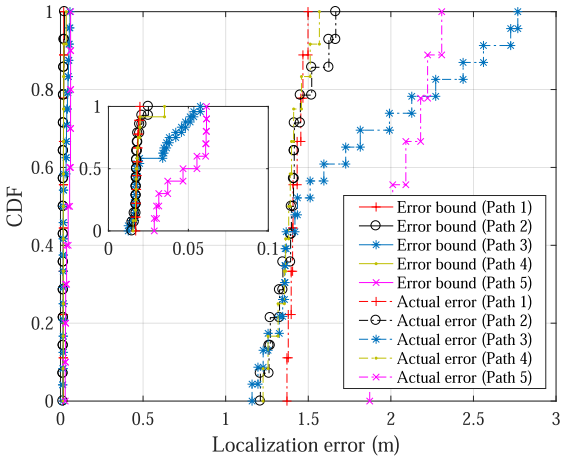

FIGURE 3. Error bound vs. actual error on different motion paths.

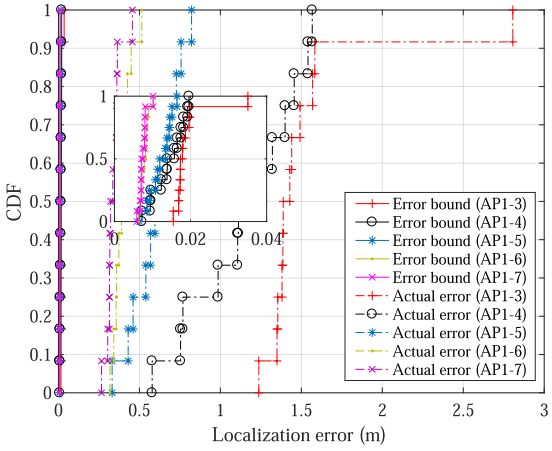

FIGURE 4. Error bound vs. actual error under different AP number.

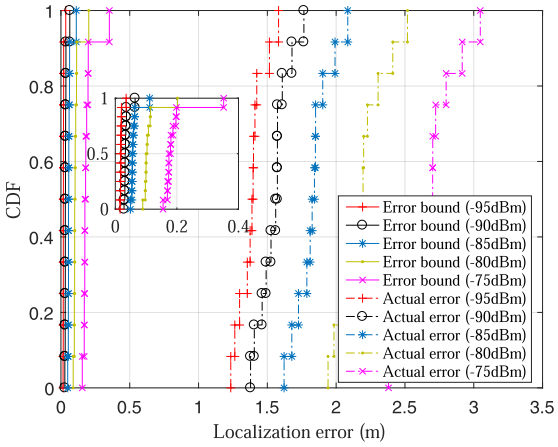

FIGURE 5. Error bound vs. actual error with different noise power.

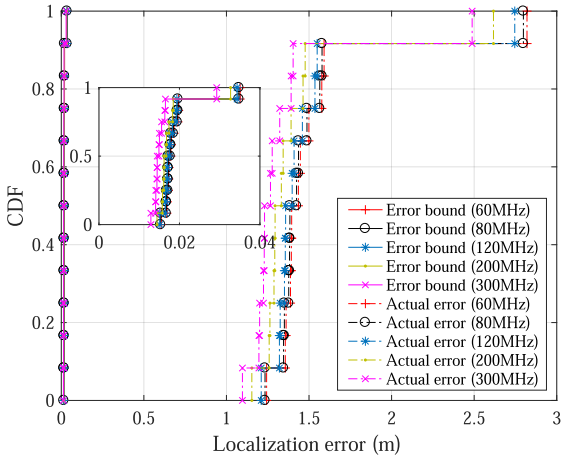

FIGURE 6. Error bound vs. actual error with different bandwidth.

The density of the AP deployment number has played a big deal towards indoor localization performance in recent years and with a fast-track trend increase. Thus, we evaluate the impact toward the error bound as in Fig. 4. Observing the CDF's, an increase of the AP number density has a positive impact on the localization performance as expected, bringing a richer CSI about characteristics of the propagation path.

Indoor environments comprise of noise power that is always time-variant and unpredictable, always considered to follow a Gaussian distribution model. The ideal use of the model in localization error bound derivation results in a distinct difference as we observe the CDF's in Fig. 5 with different noise power. This result indicates that with the increase of the noise power, both the local error bound and the actual error towards localization increase with the similar variation trend.

The increase of the bandwidth toward both the localization error bound and the actual error show the downward trend as observed in Fig. 6 CDF's, due to the fact that an increase of the bandwidth improves the time resolution ability of the AP for discriminating directions of the received multi-path signals.

B. IMPACT OF THE DEPLOYMENT OF APs

In order to future verify the proposed localization error bound, we compare the localization error under different APs distribution (symmetric distribution shown in 7(a), linear distribution shown in 7(b), minimize error bound distribution shown in 7(c)). As shown in 7(d), the value of the localizaiton error bound under the linear distribution is the largest, and then APs is deployed based on the proposed localizaiton error bound which minimizes the value of error bound. The 7(e) shows that the actual localization error is consistent with the correspond APs deployment. The result also shows that the derived error bound can be used to guide the APs deployment to optimize localization system leveraging pedestrian random motion.

C. IMPACT OF ASYNCHRONOUS EFFECT ON ERROR BOUND

Fig. 8(a) and Fig. 8(b) show localization error bound and the actual localization error with the clock synchronization and asynchronization, respectively. It can be observed that the clock asynchronous effect has a negative impact on

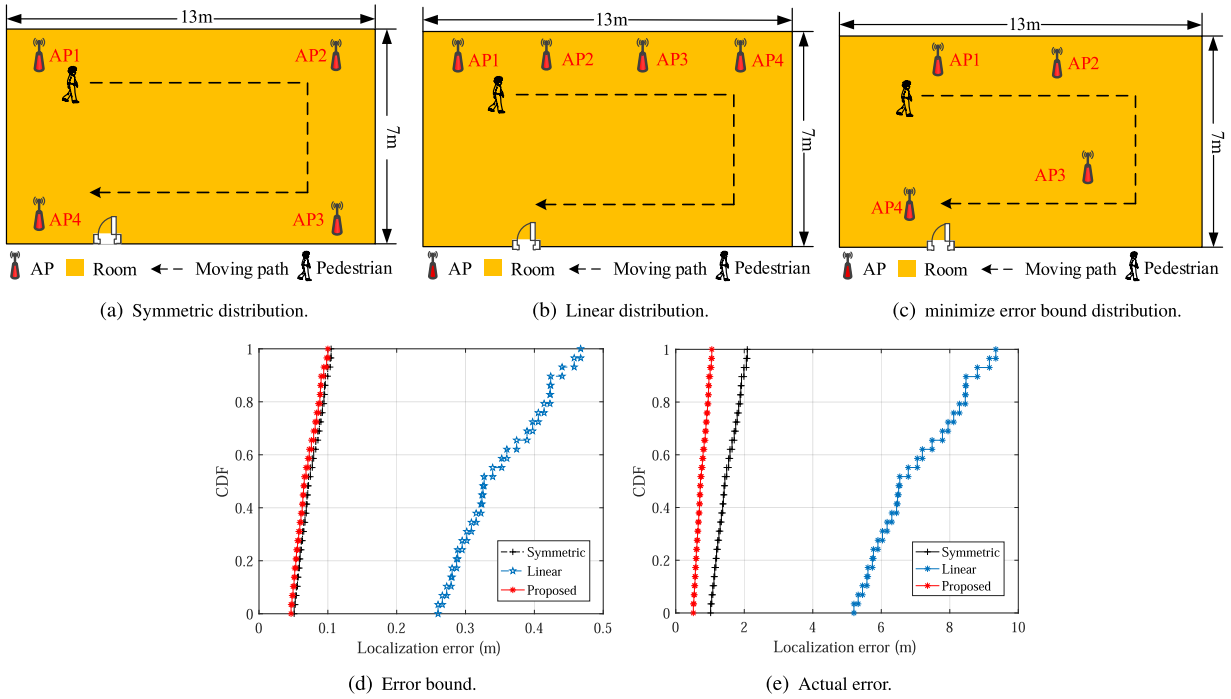

(a) Symmetric distribution. (b) Linear distribution. (c) minimize error bound distribution.

(d) Error bound. (e) Actual error.

FIGURE 7. **Impact of the geometry of APs.**

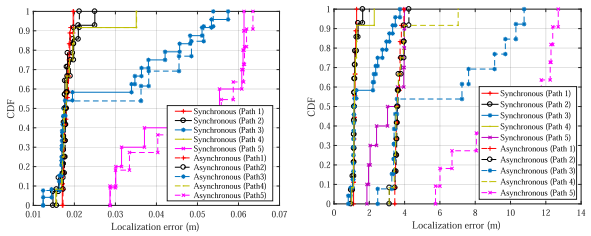

(a) Error bound (b) Actual error

FIGURE 8. **Error bound vs. actual error under clock synchronization and ansychronization.**

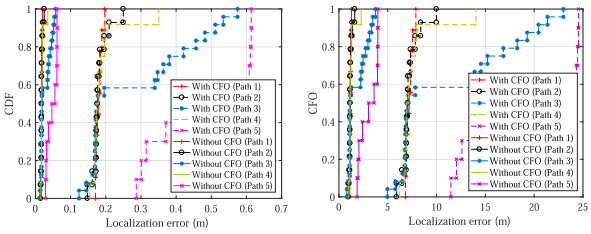

(a) Error bound (b) Actual error

FIGURE 9. **Error bound vs. actual error with CFO and without CFO.**

the localization accuracy, especially in the actual environment. Therefore, the clock asynchronous effect should be eliminated as much as possible to achieve high-precision localization.

Fig. 9(a) and Fig. 9(b) show localization error bound and the actual localization error with the CFO and without the CFO, respectively. It can be seen observed the proposed localization error bound can effectively show the impact of CFO on error bound, and Meanwhile, it also shows that the CFO will seriously affect the localization accuracy. Therefore, the CFO also should be eliminated as much as possible to achieve high-precision localization.

VII. CONCLUSION

This paper proposes the closed-form solution to the CSI-based indoor localization error bound, verified to investigate the ideal performance of indoor pedestrian localization methods. Experimental results in a real indoor environment demonstrate the effectiveness of the derived localization error bound compared to the existing localization error based on different environment and device factors. The derived localization error bound can be used to guide the AP deployment to optimize localizaiton system leveraging pedestrian random motion.

REFERENCES

[1] T.-H. Chang, L.-S. Wang, and F.-R. Chang, "A solution to the ill-conditioned GPS positioning problem in an urban environment," *IEEE Trans. Intell. Transp. Syst.*, vol. 10, no. 1, pp. 135–145, Mar. 2009.

[2] M. Zhou, Y. Wang, Z. Tian, Y. Lian, Y. Wang, and B. Wang, "Calibrated data simplification for energy-efficient location sensing in Internet of Things," *IEEE Internet Things J.*, vol. 6, no. 4, pp. 6125–6133, Aug. 2019.

[3] M. Ture and A. Hatipoglu, "Indoor location finding of the transmitter based on Bluetooth received signal strength," in *Proc. Int. Symp. Netw., Comput. Commun. (ISNCC)*, Jun. 2019, pp. 1–5.

[4] J. Su, A. X. Liu, Z. Sheng, and Y. Chen, "A partitioning approach to RFID identification," *IEEE/ACM Trans. Netw.*, early access, Jul. 10, 2020, doi: 10.1109/TNET.2020.3004852.

[5] J. Su, Y. Chen, Z. Sheng, Z. Huang, and A. X. Liu, "From M-ary query to bit query: A new strategy for efficient large-scale RFID identification," *IEEE Trans. Commun.*, vol. 68, no. 4, pp. 2381–2393, Apr. 2020.

[6] S.-H. Fang, C.-H. Wang, T.-Y. Huang, C.-H. Yang, and Y.-S. Chen, "An enhanced ZigBee indoor positioning system with an ensemble approach," *IEEE Commun. Lett.*, vol. 16, no. 4, pp. 564–567, Apr. 2012.

[7] W. You, F. Li, L. Liao, and M. Huang, "Data fusion of UWB and IMU based on unscented Kalman filter for indoor localization of quadrotor UAV," *IEEE Access*, vol. 8, pp. 64971–64981, 2020.

[8] M. Zhou, Y. Liu, Y. Wang, and Z. Tian, "Anonymous crowdsourcing-based WLAN indoor localization," *Digit. Commun. Netw.*, vol. 5, no. 4, pp. 226–236, Nov. 2019.

[9] J. Su, Z. Sheng, A. X. Liu, Z. Fu, and Y. Chen, "A time and energy saving-based frame adjustment strategy (TES-FAS) tag identification algorithm for UHF RFID systems," *IEEE Trans. Wireless Commun.*, vol. 19, no. 5, pp. 2974–2986, May 2020.

[10] J. Su, Z. Sheng, A. X. Liu, Y. Han, and Y. Chen, "A group-based binary splitting algorithm for UHF RFID anti-collision systems," *IEEE Trans. Commun.*, vol. 68, no. 2, pp. 998–1012, Feb. 2020.

[11] A. Achroufene, Y. Amirat, and A. Chibani, "RSS-based indoor localization using belief function theory," *IEEE Trans. Autom. Sci. Eng.*, vol. 16, no. 3, pp. 1163–1180, Jul. 2019.

[12] W. Liu, Q. Cheng, Z. Deng, H. Chen, X. Fu, X. Zheng, S. Zheng, C. Chen, and S. Wang, "Survey on CSI-based indoor positioning systems and recent advances," in *Proc. Int. Conf. Indoor Positioning Indoor Navigat. (IPIN)*, Sep. 2019, pp. 1–8.

[13] M. Zheng, S. Li, L. Deng, M. Qu, C. Zhang, and C. Cai, "CSI-based indoor high-precision localization system," in *Proc. Asia–Pacific Microw. Conf. (APMC)*, Nov. 2018, pp. 357–359.

[14] G. Yang, "WiLocus: CSI based human tracking system in indoor environment," in *Proc. 8th Int. Conf. Measuring Technol. Mechatronics Autom. (ICMTMA)*, Mar. 2016, pp. 915–918.

[15] X. Liu, C. Sun, M. Zhou, C. Wu, B. Peng, and P. Li, "Reinforcement learning-based multislot double-threshold spectrum sensing with Bayesian fusion for industrial big spectrum data," *IEEE Trans. Ind. Informat.*, early access, Apr. 15, 2020, doi: 10.1109/TII.2020.2987421.

[16] W.-K. Yang, C.-M. Shen, and T.-H. Sang, "PASTd-based CSI tracking in massive MIMO systems," in *Proc. IEEE 23rd Int. Conf. Digit. Signal Process. (DSP)*, Nov. 2018, pp. 1–5.

[17] M. Kotaru, K. Joshi, D. Bharadia, and S. Katti, "SpotFi: Decimeter level localization using WiFi," *ACM SIGCOMM Comput. Commun. Rev.*, vol. 45, no. 4, pp. 269–282, Sep. 2015.

[18] S. Kumar, S. Gil, D. Katabi, and D. Rus, "Accurate indoor localization with zero start-up cost," in *Proc. 20th Annu. Int. Conf. Mobile Comput. Netw. (MobiCom)*, Sep. 2014, pp. 483–494.

[19] S. Shi, S. Sigg, L. Chen, and Y. Ji, "Accurate location tracking from CSI-based passive device-free probabilistic fingerprinting," *IEEE Trans. Veh. Technol.*, vol. 67, no. 6, pp. 5217–5230, Jun. 2018.

[20] H. Liu, N. Xia, D. Guo, and P. Qing, "CSI-based indoor tracking with positioning-assisted," in *Proc. Ubiquitous Positioning, Indoor Navigat. Location-Based Services (UPINLBS)*, Mar. 2018, pp. 1–8.

[21] H. Yu, G.-L. Chen, G.-J. Yu, S.-H. Zhao, B. Yang, and J. Liu, "Indoor passive localisation based on reliable CSI extraction," *IET Commun.*, vol. 13, no. 11, pp. 1633–1642, Jul. 2019.

[22] H. Yu, B. Yang, J. Liu, and G.-J. Yu, "Passive human trajectory tracking study in indoor environment with CSI," in *Proc. Int. Conf. Netw. Netw. Appl. (NaNA)*, Oct. 2018, pp. 372–377.

[23] H. Choi, S. Son, J. Kim, and Y. Baek, "RF-based indoor locating system for NLOS environment," in *Proc. 24th IEEE Int. Conf. Adv. Inf. Netw. Appl.*, Apr. 2010, pp. 628–633.

[24] Y. Ma, B. Wang, S. Pei, Y. Zhang, S. Zhang, and J. Yu, "An indoor localization method based on AOA and PDOA using virtual stations in multipath and NLOS environments for passive UHF RFID," *IEEE Access*, vol. 6, pp. 31772–31782, 2018.

[25] S. Li, M. Hedley, I. B. Collings, and D. Humphrey, "Joint trajectory and ranging offset estimation for accurate tracking in NLOS environments," *IEEE Trans. Aerosp. Electron. Syst.*, vol. 56, no. 1, pp. 3–14, Feb. 2020.

[26] H. Rahul, S. Kumar, and D. Katabi, "JMB: Scaling wireless capacity with user demands," *ACM SIGCOMM Comput. Commun. Rev.*, vol. 42, no. 4, pp. 235–246, 2012.

[27] L. Wu, X.-D. Zhang, P.-S. Li, and Y.-T. Su, "A closed-form blind CFO estimator based on frequency analysis for OFDM systems," *IEEE Trans. Commun.*, vol. 57, no. 6, pp. 1634–1637, Jun. 2009.

[28] J. Ma, J. He, M. Chen, Z. Zhou, Y. Liu, Y. Xiao, and Y. Cheng, "Cost-effective SFO compensation scheme based on TSs for OFDM-PON," *IEEE/OSA J. Opt. Commun. Netw.*, vol. 11, no. 6, pp. 299–306, Jun. 2019.

[29] B. Xie, W. Qiu, and H. Minn, "Exact signal model and new carrier frequency offset compensation scheme for OFDM," *IEEE Trans. Wireless Commun.*, vol. 11, no. 2, pp. 550–555, Feb. 2012.

[30] J. Yuan and M. Torlak, "Joint CFO and SFO estimator for OFDM receiver using common reference frequency," *IEEE Trans. Broadcast.*, vol. 62, no. 1, pp. 141–149, Mar. 2016.

[31] M. Zhou, Y. Wang, Y. Liu, and Z. Tian, "An information-theoretic view of WLAN localization error bound in GPS-denied environment," *IEEE Trans. Veh. Technol.*, vol. 68, no. 4, pp. 4089–4093, Apr. 2019.

[32] M. Zhou, F. Qiu, K. Xu, Z. Tian, and H. Wu, "Error bound analysis of indoor Wi-Fi location fingerprint based positioning for intelligent access point optimization via Fisher information," *Comput. Commun.*, vol. 86, pp. 57–74, Jul. 2016.

[33] L. Gui, M. Yang, H. Yu, J. Li, F. Shu, and F. Xiao, "A Cramer–Rao lower bound of CSI-based indoor localization," *IEEE Trans. Veh. Technol.*, vol. 67, no. 3, pp. 2814–2818, Mar. 2018.

[34] X. Tian, S. Zhu, S. Xiong, B. Jiang, Y. Yang, and X. Wang, "Performance analysis of Wi-Fi indoor localization with channel state information," *IEEE Trans. Mobile Comput.*, vol. 18, no. 8, pp. 1870–1884, Aug. 2019.

[35] W. Croswell, "Antenna theory, analysis, and design," *IEEE Antennas Propag. Soc. Newslett.*, vol. 24, no. 6, pp. 28–29, Dec. 1982.

[36] S. M. Kay, "Fundamentals of statistical signal processing," *Technometrics*, vol. 37, no. 4, pp. 465–466, 1993.

[37] J. Xiong and K. Jamieson, "ArrayTrack: A fine-grained indoor location system," in *Proc. 10th USENIX Conf. Netw. Syst. Design Implement.*, 2013, pp. 71–84.

[38] Y. Xie, Z. Li, and M. Li, "Precise power delay profiling with commodity Wi-Fi," *IEEE Trans. Mobile Comput.*, vol. 18, no. 6, pp. 1342–1355, Jun. 2019.

[39] Y. Shen and M. Z. Win, "Fundamental limits of wideband Localization—Part I: A general framework," *IEEE Trans. Inf. Theory*, vol. 56, no. 10, pp. 4956–4980, Oct. 2010.

[40] T. Pollet, M. Van Bladel, and M. Moeneclaey, "BER sensitivity of OFDM systems to carrier frequency offset and Wiener phase noise," *IEEE Trans. Commun.*, vol. 43, nos. 2–4, pp. 191–193, Feb. 1995.

ZHENYA ZHANG received the B.S. degree in telecommunication engineering from the North China University of Water Resources and Electric Power, in 2018. He is currently pursuing the M.S. degree in information and communication engineering with the Chongqing University of Posts and Telecommunications (CQUPT). His current research interests include indoor localization, fisher information matrix, and CRLB.

WEI NIE received the Ph.D. degree from the University of Electronic Science and Technology of China (UESTC), Chengdu, China, in 2015. From 2015 to 2016, he worked as an Engineer at Huawei. Since August 2016, he has been working as a Lecturer with the Chongqing University of Posts and Telecommunications (CQUPT), Chongqing, China. His current research area includes microwave and mm-wave passive devices and antenna technology.

YONG WANG (Member, IEEE) received the B.S., M.S., and Ph.D. degrees from the Harbin Institute of Technology, Harbin, China, in 2010, 2012, and 2018, respectively. He is currently a Lecturer with the Chongqing University of Posts and Telecommunications, Chongqing, China. From January 2014 to June 2015, he was a Visiting Ph.D. Student with the Department of Electrical and Computer Engineering, University of Toronto, Canada. His research interests include resource allocation and signal processing in cooperative networks, deep learning, and WiFi localization.

LIANGBO XIE (Member, IEEE) received the B.S. and M.S. degrees from Chongqing University, in 2007 and 2010, respectively, and the Ph.D. degree from the University of Electronic Science and Technology of China (UESTC), in 2016. He is currently an Associate Professor with the School of Communication and Information Engineering, Chongqing University of Posts and Telecommunications, Chongqing, China. His research interests include ultra-low-power analog circuits, low-power SAR ADC, low-power digital circuits, anti-collision Algorithm for RFID, and indoor-localization.